

Observational constraints on models of the Universe with time variable Gravitational and Cosmological constants along MOG

M. Khurshudyan,¹ N. S. Mazhari,² D. Momeni,² R. Myrzakulov,² and M. Raza^{3,4}

¹*Department of Theoretical Physics, Yerevan State University,*

1 Alex Manookian, 0025, Yerevan, Armenia

²*Eurasian International Center for Theoretical Physics,*

Eurasian National University, Astana 010008, Kazakhstan

³*Department of Mathematics, COMSATS Institute of Information Technology, Sahiwal, Pakistan*

⁴*Centre for Optical and Electromagnetic Research,*

Department of Electrical Engineering, Zhejiang University, Hangzhou, China

The subject of this paper is to investigate the weak regime covariant scalar-tensor-vector gravity (STVG) theory, known as the MODified gravity (MOG) theory of gravity. First, we show that the MOG in the absence of scalar fields is converted into $\Lambda(t), G(t)$ models. Time evolution of the cosmological parameters for a family of viable models have been investigated. Numerical results with the cosmological data have been adjusted. We've introduced a model for dark energy (DE) density and cosmological constant which involves first order derivatives of Hubble parameter. To extend this model, correction terms including the gravitational constant are added. In our scenario, the cosmological constant is a function of time. To complete the model, interaction terms between dark energy and dark matter (DM) manually entered in phenomenological form. Instead of using the dust model for DM, we have proposed DM equivalent to a barotropic fluid. Time evolution of DM is a function of other cosmological parameters. Using sophisticated algorithms, the behavior of various quantities including the densities, Hubble parameter, etc. have been investigated graphically. The statefinder parameters have been used for the classification of DE models. Consistency of the numerical results with experimental data of $SneIa + BAO + CMB$ are studied by numerical analysis with high accuracy.

PACS numbers: 98.80.Es, 95.36.+x, 04.80.-y, 06.20.Jr, 95.30.Ft

Keywords: Dark energy, Cosmological constant, Gravitational constant

I. A NEW SYNTHESIS OF TIME VARIABLE G, Λ MODELS AS MOG MODELS

All Cosmological data from different sources testify to the fact that our world is made of a substance of negative pressure 73% (dark energy (DE)), missing mass 23% (dark matter (DM)) and only 4% conductive material (baryon matter) [1]. DM and DE can have interaction and the interaction of these is not known in the physics. It is not an electromagnetic field and metallic material interaction. Mathematical function is determined phenomenologically because types of interactions is unknown with an overall classification interaction function can be written as $Q = Q(H, \dot{H}, \rho_m, \rho_{DE}, \rho_{DM}, \dots)$.

Several models have been proposed to explain the universe's accelerated expansion [4]-[10]. The models can be divided into two general groups: the first group of models that are needed to correct the Einstein theory of gravity with a new geometric terms is known as geometric models. The first of these models is $f(R)$ which is obtained by replacing the R Ricci curvature with arbitrary $f(R)$ function[11]. The second group of models that are expansion is attributed to exotic fluids with negative pressure. It is believed that exotic fluid is a mimic dark energy equation of state in the present era (for a modern review see [2],[3]). Both of these models have different applications and important results of these models are derived as alternative cosmological models [12–16].

Several properties of DE have been studied in numerous papers[17–19]. DE can be decay [20] or reconstruct from different theoretical models [21]. There is no simple and unique model that can have to describe this exotic energy. Models in which the Scalar-tensor fields used are able to solve such complex issues by simple mathematics to the extend possible [22, 23]. So there are very attractive models to study. A scalar-Tensor model is proposed among all the different cosmological models. The model is able to explain the DM and dynamic clusters of galaxies with an additional vector field and relying only baryonic matter [24]. This model is known as STVG or MOG. MOG can be seen as a covariant theory with vector-tensor-scalar fields for gravity with the following action:

$$S = -\frac{1}{16\pi} \int \frac{1}{G}(R + 2\Lambda)\sqrt{-g}d^4x + S_\phi + S_M \quad (1)$$

$$- \int \frac{1}{G} \left[\frac{1}{2} g^{\alpha\beta} \left(\nabla_\alpha \log G \nabla_\beta \log G + \nabla_\alpha \log \mu \nabla_\beta \log \mu \right) + U_G(G) + W_\mu(\mu) \right] \sqrt{-g}d^4x.$$

The first term of the action is Einstein-Hilbert Lagrangian. The second term is the conventional

scalar field and the last term contains a G kinetic energy field that plays the role of the gravitational constant (However, the fields can be considered similar to a time dependent gravitational constant by slowly time varying fields) [25]. This action classes are written in covariant forms and are used to investigate the astrophysical phenomena such as rotation curves of galaxies, mass distribution of cosmic clusters or gravitational lenses. The model might be a suitable alternative to Λ CDM model considered [26]. In order to understand the role of scalar and vector fields we write the equations of motion for FLRW metric :

$$ds^2 = dt^2 - a(t)^2[(1 - kr^2)^{-1}dr^2 + r^2d\Omega^2], \quad d\Omega^2 = d\theta^2 + \sin^2\theta d\phi^2$$

Form of the equations can be rewritten as a generalized Friedmann equations as follow [27]:

$$H^2 + \frac{k}{a^2} = \frac{8\pi G\rho}{3} - \frac{4\pi}{3} \left(\frac{\dot{G}^2}{G^2} + \frac{\dot{\mu}^2}{\mu^2} - \dot{\omega}^2 - G\omega\mu^2\phi_0^2 \right) + \frac{8\pi}{3} \left(\omega GV_\phi + \frac{V_G}{G^2} + \frac{V_\mu}{\mu^2} + V_\omega \right) + \frac{\Lambda}{3} + H \frac{\dot{G}}{G}, \quad (2)$$

$$\begin{aligned} \frac{\ddot{a}}{a} = & -\frac{4\pi G}{3}(\rho + 3p) + \frac{8\pi}{3} \left(\frac{\dot{G}^2}{G^2} + \frac{\dot{\mu}^2}{\mu^2} - \dot{\omega}^2 - G\omega\mu^2\phi_0^2 \right) \\ & + \frac{8\pi}{3} \left(\omega GV_\phi + \frac{V_G}{G^2} + \frac{V_\mu}{\mu^2} + V_\omega \right) + \frac{\Lambda}{3} + H \frac{\dot{G}}{2G} + \frac{\ddot{G}}{2G} - \frac{\dot{G}^2}{G^2}, \\ \ddot{G} + 3H\dot{G} - \frac{3}{2} \frac{\dot{G}^2}{G} + \frac{G}{2} \left(\frac{\dot{\mu}^2}{\mu^2} - \dot{\omega}^2 \right) + \frac{3}{G} V_G - V'_G \\ & + G \left[\frac{V_\mu}{\mu^2} + V_\omega \right] + \frac{G}{8\pi} \Lambda - \frac{3G}{8\pi} \left(\frac{\ddot{a}}{a} + H^2 \right) = 0, \end{aligned} \quad (3)$$

$$\ddot{\mu} + 3H\dot{\mu} - \frac{\dot{\mu}^2}{\mu} - \frac{\dot{G}}{G}\dot{\mu} + G\omega\mu^3\phi_0^2 + \frac{2}{\mu}V_\mu - V'_\mu = 0, \quad (4)$$

$$\ddot{\omega} + 3H\dot{\omega} - \frac{\dot{G}}{G}\dot{\omega} - \frac{1}{2}G\mu^2\phi_0^2 + GV_\phi + V'_\omega = 0. \quad (5)$$

Scalar and vector fields interaction terms of the aforementioned classes are self interaction and they are shown by an arbitrary mathematical functions: $V_\phi(\phi)$, $V_G(G)$, $V_\omega(\omega)$, and $V_\mu(\mu)$. The resulting equations of motion are highly nonlinear and there is no possibility to find analytical solutions. The only possible way to evaluate answer is numerical method. At the same time, we must also determine the shape of the interaction V_i . Mathematical differences may be a good solution for finding certain family of potentials. If we consider the G scalar field with a time variable gravitational field ($G(t)$) and ignore the contributions of the other fields in favor of the $G(t)$, and also due to the cosmological data $\frac{\dot{G}}{G} \ll 1$, time evolution of $G(t)$ will be the major contribution.

In fact, data from the large cosmological confirm our conjecture about just keeping the $G(t)$, and kinetic part of $G(t)$ can be neglected because:

$$g^{\alpha\beta}\nabla_\alpha\log G\nabla_\beta\log G\simeq(\frac{\dot{G}}{G})^2\ll 1. \quad (6)$$

Regardless, second-order derivatives of additional fields which introduced additional degrees of freedom and in the absence of additional fields on MOG, with the approximation that the time evolution of the fields is very slowly varying, MOG and Einstein-Hilbert action can be considered as the same. The difference is that now $G(t)$ is a scalar time variable field. Equations of motion are written in the following general form, if we consider small variation of $G(t)$ and $G(t), \Lambda$ are functions of time [28]:

$$S\simeq -\frac{1}{16\pi}\int\frac{1}{G}(R+2\Lambda)\sqrt{-g}d^4x+S_M. \quad (7)$$

(see for instance [29])

$$R_{\mu\nu}-\frac{1}{2}Rg_{\mu\nu}\approx-8\pi G(t)\left[T_{\mu\nu}-\frac{\Lambda(t)}{8\pi G(t)}g_{\mu\nu}\right], \quad (8)$$

Energy-momentum function of matter fields (ordinary or exotic) is proposed as follows:

$$T_{\mu\nu}=\mathcal{L}_Mg_{\mu\nu}-2\frac{\delta\mathcal{L}_M}{\delta g^{\mu\nu}}. \quad (9)$$

Cosmological models, which were introduced by the mentioned equations of motion have been investigated several times by different authors [29–32]. But we approach this problem with a more general view. As we have shown, MOG is the limit of weak fields able to induce and introduces a gravitational field $G(t)$. So, our paper can be considered as a cosmological analysis of MOG in the weak field regime. We are particularly interested to see how cosmological data *SneIa + BAO + CIB* will constrain our model parameters.

Our plan in this paper is: In section II: introducing the cosmological constant and dark model consist of $\{H, \dot{H}, ..\}$. In section III: dynamic extraction of the model and additional equation governing $G(t)$ and inference different densities. In section IV, numerical analysis of the equations. In section V, statefinder parameters (r, s) analysis. In section VI, observational constraints. The final section is devoted to the results of references.

II. TOY MODELS

A DE model of our interest is described via energy density ρ_D [33]:

$$\rho_D = \alpha \frac{\ddot{H}}{H} + \beta \dot{H} + \gamma H^2, \quad (10)$$

where β, γ are positive constants, while for α in light of the time variable scenario, we suppose that

$$\alpha(t) = \alpha_0 + \alpha_1 G(t) + \alpha_2 t \frac{\dot{G}(t)}{G(t)}, \quad (11)$$

where α_0, α_1 and α_2 are positive constants and $G(t)$ is a varying gravitational constant. Its a generalization of Ricci dark energy scenario [34] to higher derivatives terms of Hubble parameter.

An interaction term Q between DE and a barotropic fluid $P_b = \omega_b \rho_b$ is taken to be

$$Q = 3Hb(\rho_b + \rho_D) \quad (12)$$

We propose three phenomenological models for DE as the following:

1. The first model is the simplest one, in which we assume that time variable cosmological constant has the same order of energy as the density of DE.

$$\Lambda(t) = \rho_D,$$

In this model, ρ_D is determined using continuity equation with a dissipative interaction term Q .

2. Secondly, generalization of cosmological constant is proposed as a modified Ricci DE model to time variable scenario has an oscillatory form in terms of H .

$$\Lambda(t) = \rho_b \sin^3(tH) + \rho_D \cos(tH),$$

Note that if we think on trigonometric term as oscillatory term, the amplitudes of the oscillations are assumed to be proportional to the barotropic and DE components. Meanwhile these coefficients satisfy continuity equations.

3. The last toy model is inspired from the small variation of $G(t)$ and a logarithmic term of H . Here, coefficients are written in the forms of barotropic and DE densities .

$$\Lambda(t) = \rho_b \ln(tH) + \rho_D \sin\left(t \frac{\dot{G}(t)}{G(t)}\right).$$

In this model, a time dependent and G variable assumption is imposed.

Following the suggested models we will study time evolution and cosmological predictions of our cosmological model. Furthermore, we will compare the numerical results with a package of observational data.

III. DYNAMIC OF MODELS

By using the following FRW metric for a flat Universe,

$$ds^2 = -dt^2 + a(t)^2 (dr^2 + r^2 d\Omega^2), \quad (13)$$

field equations (8) can be reduced to the following Friedmann equations,

$$H^2 = \frac{\dot{a}^2}{a^2} = \frac{8\pi G(t)\rho}{3} + \frac{\Lambda(t)}{3}, \quad (14)$$

and,

$$\frac{\ddot{a}}{a} = -\frac{4\pi G(t)}{3}(\rho + 3P) + \frac{\Lambda(t)}{3}, \quad (15)$$

where $d\Omega^2 = d\theta^2 + \sin^2 \theta d\phi^2$, and $a(t)$ represents the scale factor.

Energy conservation law $T_{ij}^{;j} = 0$ reads as,

$$\dot{\rho} + 3H(\rho + P) = 0. \quad (16)$$

Combination of (14), (15) and (16) gives the relationship between $\dot{G}(t)$ and $\dot{\Lambda}(t)$

$$\dot{G} = -\frac{\dot{\Lambda}}{8\pi\rho}. \quad (17)$$

To introduce an interaction between DE and DM (16) we should mathematically split it into two following equations

$$\dot{\rho}_{DM} + 3H(\rho_{DM} + P_{DM}) = Q, \quad (18)$$

and

$$\dot{\rho}_{DE} + 3H(\rho_{DE} + P_{DE}) = -Q. \quad (19)$$

For the barotropic fluid with $P_b = \omega_b \rho_b$ (18) will take following form

$$\dot{\rho}_b + 3H(1 + \omega_b - b)\rho_b = 3Hb\rho_D. \quad (20)$$

Pressure of the DE can be recovered from (19)

$$P_D = -\rho_D - \frac{\dot{\rho}_D}{3H} - b \frac{3H^2 - \Lambda(t)}{8\pi G(t)}. \quad (21)$$

Therefore with a fixed form of $\Lambda(t)$ we will be able to observe behavior of P_D . Cosmological parameters of our interest are EoS parameters of DE $\omega_D = P_D/\rho_D$, EoS parameter of composed fluid

$$\omega_{tot} = \frac{P_b + P_D}{\rho_b + \rho_D},$$

deceleration parameter q , which can be written as

$$q = \frac{1}{2} \left(1 + 3 \frac{P}{\rho} \right), \quad (22)$$

where $P = P_b + P_D$ and $\rho = \rho_b + \rho_D$. We have a full system of equations of motion and interaction terms. Now we are ready to investigate cosmological predictions of our model.

IV. NUMERICAL ANALYSIS OF THE COSMOLOGICAL PARAMETERS

In next sections we fully analyze time evolution of three models of DE. Using numerical integration, we will show that how cosmological parameters $H, G(t), q, w_{tot}$, and time decay rate $\frac{d \log G}{dt}$ and densities ρ_D, \dots change. We fit parameters like H_0 , etc from observational data.

A. Model 1: $\Lambda(t) = \rho_D$

In this section we will consider $\Lambda(t)$ to be of the form

$$\Lambda(t) = \rho_D. \quad (23)$$

Therefore for the pressure of DE we will have

$$P_D = \left(\frac{b}{8\pi G(t)} - 1 \right) \rho_D - \frac{\dot{\rho}_D}{3H} - \frac{3b}{8\pi G(t)} H^2. \quad (24)$$

The dynamics of $G(t)$ we will have

$$\frac{\dot{G}(t)}{G(t)} + \frac{\dot{\rho}_D}{3H^2 - \rho_D} = 0. \quad (25)$$

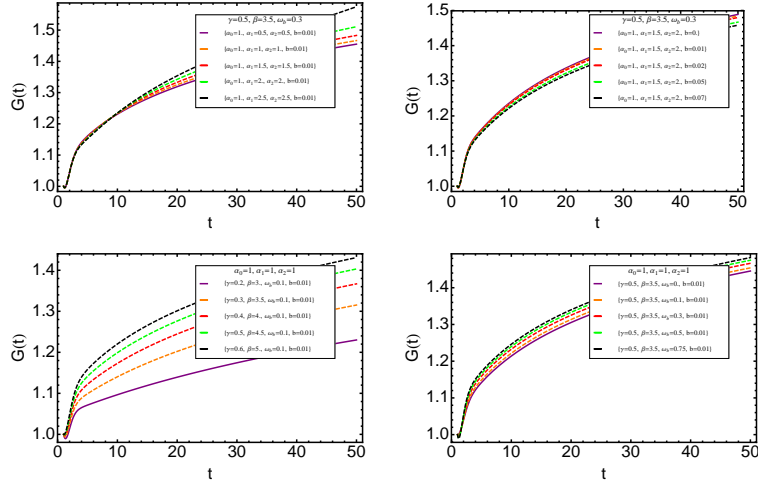
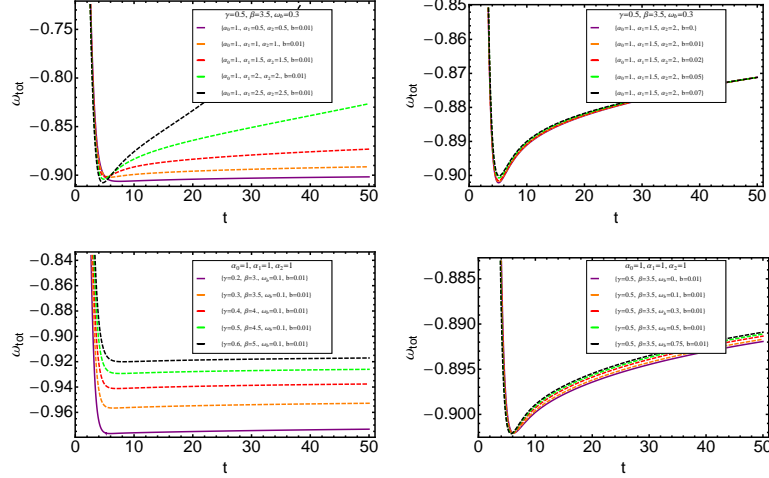
Performing a numerical analysis for the general case we recover the graphical behavior of different cosmological parameters. Graphical behavior of Gravitational constant $G(t)$ against time t presented

in Fig.(1). We see that $G(t)$ is an increasing function. Different plots represent behavior of $G(t)$ as a function of the parameters of the model. For this model with the specific behavior of $G(t)$ for Hubble parameter H gives decreasing behavior over time. It is confirmed by LCDM scenario. From the analysis of the graphical behavior of ω_{tot} we made the following conclusion that with $\alpha_0 = 1$, $\gamma = 0.5$, $\beta = 3.5$, $\omega_b = 0.3$, $b = 0.01$ (interaction parameter) and with increasing α_1 and α_2 we increase the value of ω_{tot} for later stages of evolution, while for the early stages, in history, it is a decreasing function. For instance, with $\alpha_1 = 0.5$ and $\alpha_2 = 0.5$ (blue line) ω_{tot} is a constant and $\omega_{tot} \approx -0.9$ (Top left plot in Fig.(2)). Top right plot of Fig.(2) presents graphical behavior of ω_{tot} against time as a function of the parameter b characterizing interaction between DE and DM. We see that for the later stages of the evolution the interaction $Q = 3hb(\rho_b + \rho_D)$ does not play any role. An existence of the interaction can be observed only for relatively early stages of evolution and when b is too much higher than the real values of it estimated from observations. The left-bottom plot shows the decreasing behavior of ω_{tot} at early stages of evolution which, while for later stages, becomes a constant. This behavior is observed for $\alpha_0 = \alpha_1 = \alpha_2 = 1$, $\omega_b = 0.1$, $b = 0.01$ and for increasing γ and β . With the increase in γ and β , we increase the value of ω_{tot} . The right-bottom plot represents behavior as a function of ω_b . In Fig.3, the graphical behavior of the deceleration parameter q is observed which is a negative quantity throughout the evolution of the Universe i.e. we have an ever accelerated Universe. Right panel (top and bottom) shows that the behavior of q does not strongly depend upon the interaction parameter b and EoS parameter ω_b . We also see that q starts its evolution from -1 and for a very short period of the history it becomes smaller than -1 , but after this $q > -1$ for ever, giving a hope that observational facts can be modeled (for later stages!). Right panel (top and bottom) represents the behavior of q for $\alpha_1 = \alpha_2$ and $\{\gamma, \beta\}$ (top and bottom) respectively. With the increase in the values of the parameters, the value of q increases. Some information about ω_D , $\Lambda(t)$ and $\dot{G}(t)/G(t)$ can be found in Appendix.

B. Model 2: $\Lambda(t) = \rho_b \sin(tH)^3 + \rho_D \cos(tH)$

For the second model we will consider the following phenomenological form of the $\Lambda(t)$

$$\Lambda(t) = \rho_b \sin(tH)^3 + \rho_D \cos(tH). \quad (26)$$

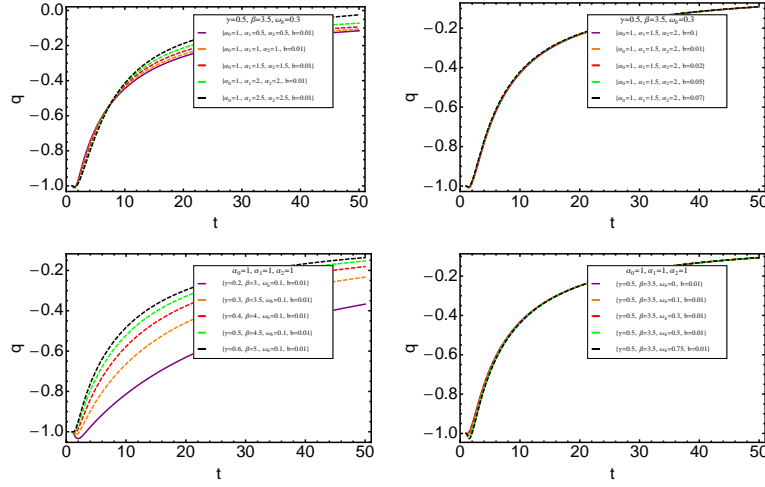
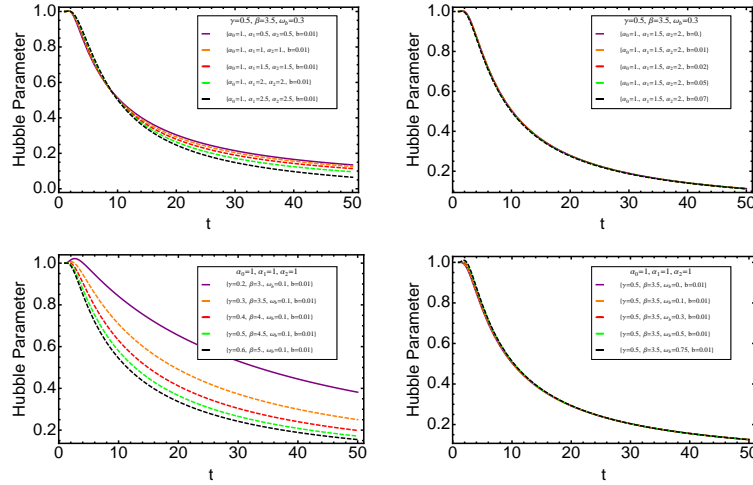
FIG. 1: Behavior of Gravitational constant $G(t)$ against t for Model 1.FIG. 2: Behavior of EoS parameter ω_{tot} against t for Model 1.

Taking into account (14) we can write $\Lambda(t)$ in a different form

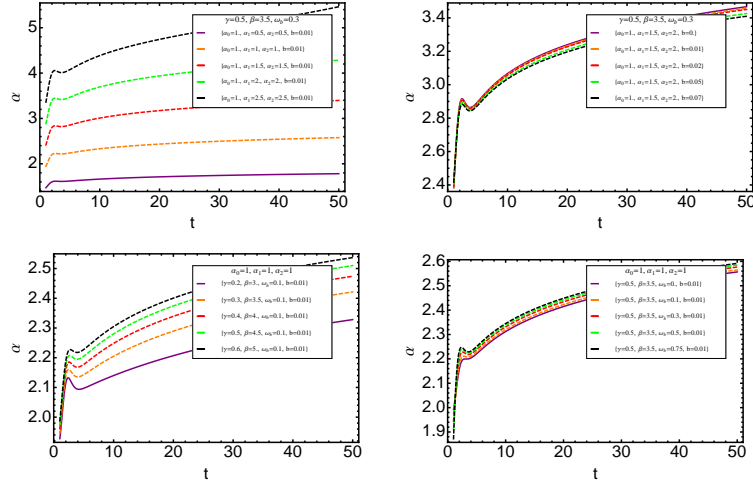
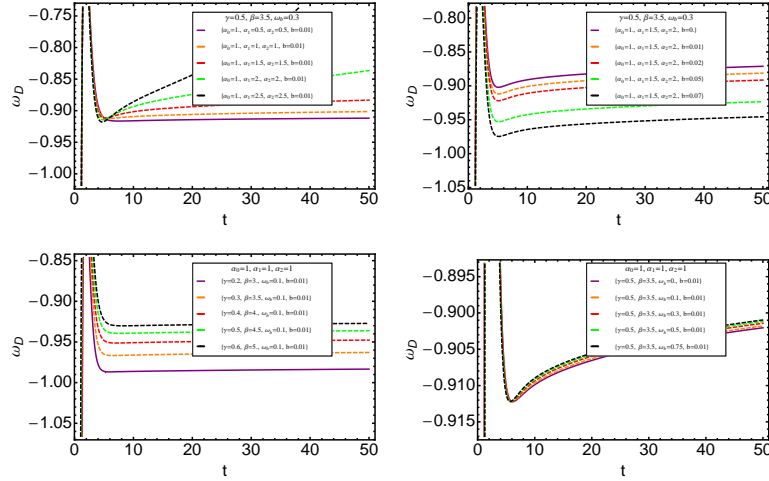
$$\Lambda(t) = \left[1 + \frac{\sin(tH)^3}{8\pi G(t)} \right]^{-1} \left(\frac{3H^2}{8\pi G(t)} \sin(tH)^3 - \rho_D(\sin(tH)^3 - \cos(tH)) \right). \quad (27)$$

$$\frac{\dot{G}(t)}{G(t)} + \frac{\dot{\Lambda}(t)}{3H^2 - \Lambda(t)} = 0, \quad (28)$$

with (30) will give us the behavior of $G(t)$ Fig(8). We see that $G(t)$ is an increasing-decreasing-increasing function (Top panel and right-bottom plot). The left-bottom plot gives us an information about the behavior of $G(t)$ as a function of γ and β with $\alpha_0 = 1$, $\alpha_1 = \alpha_2 = 1.5$ and $\omega_b = 0.3$, $b = 0.01$. We see that with increasing γ and β we are able to change the behavior of $G(t)$. For instance, with

FIG. 3: Behavior of deceleration parameter q against t for Model 1.FIG. 4: Behavior of Hubble parameter $H(t)$ against t for Model 1.

$\gamma = 0.5$ and $\beta = 3.5$ which is a blue line, still preserves the increasing-decreasing-increasing behavior. While for higher values of the parameters, we change the behavior of $G(t)$ compared to the other cases within this model and we have increasing-decreasing behavior. Graphical behavior of ω_{tot} can be found in Fig.9. The behavior of the deceleration parameter q for this model gives us almost the same as for Model 1, where $\Lambda(t) = \rho_D$. We also see that with increasing γ and β we increase the value of q (left-bottom plot). The presence of the interaction Q and the barotropic fluid for which EoS parameter $\omega_b < 1$ does not leave a serious impact on the behavior of q . This model with this behavior of $q > -1$ can be comparable with the observational facts.

FIG. 5: Behavior of α against t for Model 1.FIG. 6: Behavior of ω_D against t for Model 1.

C. Model 3: $\Lambda(t) = \rho_b \ln(tH) + \rho_D \sin\left(t \frac{\dot{G}(t)}{G(t)}\right)$

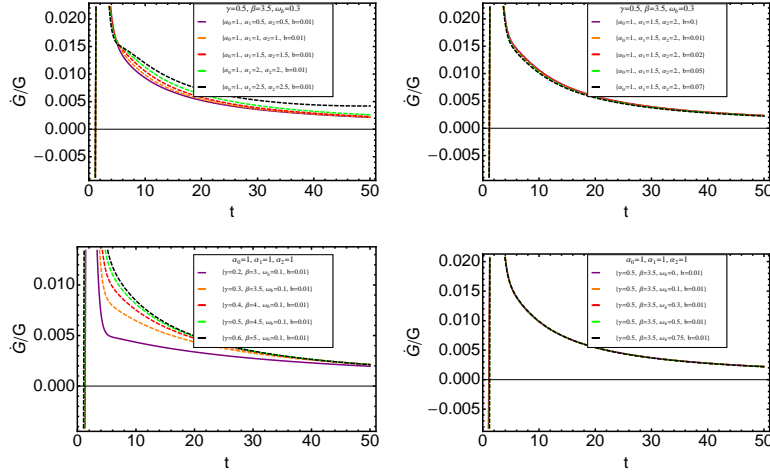
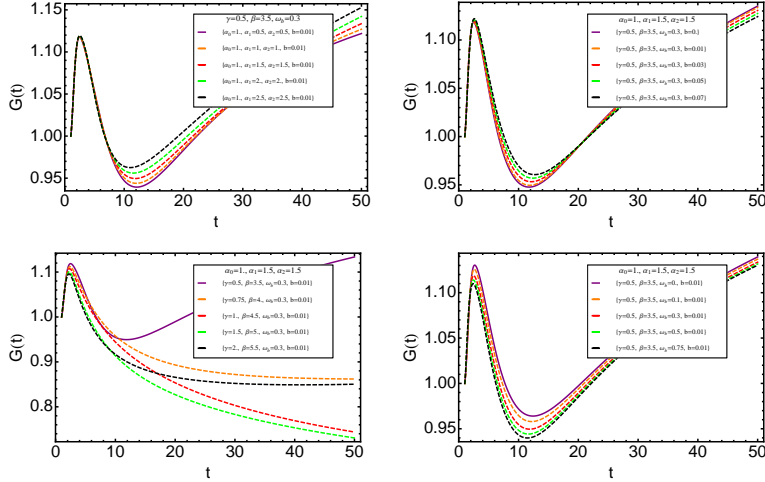
For this model we will consider the following phenomenological form of the $\Lambda(t)$

$$\Lambda(t) = \rho_b \ln(tH) + \rho_D \sin\left(t \frac{\dot{G}(t)}{G(t)}\right). \quad (29)$$

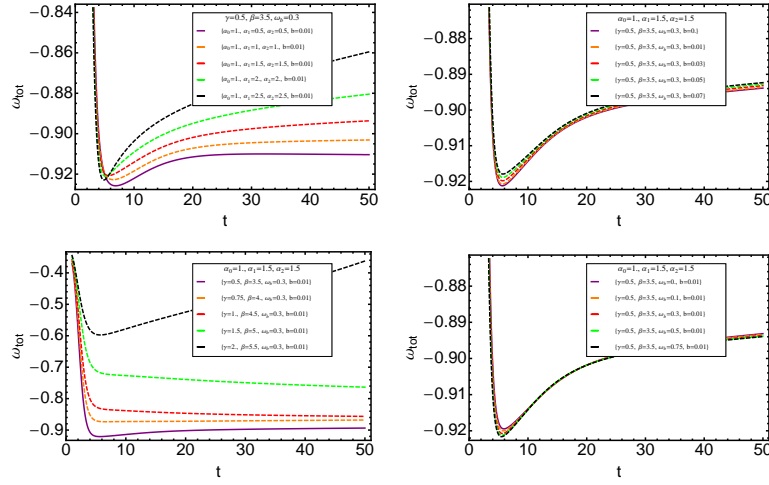
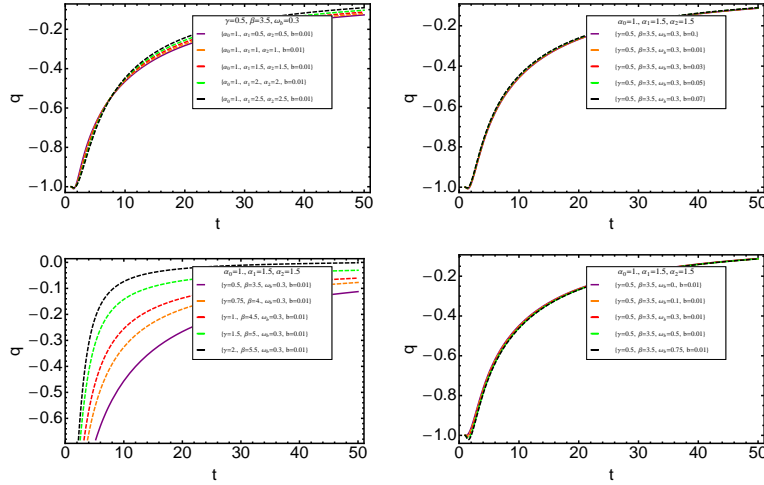
Taking into account (14) we can write $\Lambda(t)$ in a different form

$$\Lambda(t) = \left[1 + \frac{\ln(tH)}{8\pi G(t)}\right]^{-1} \left(\frac{3H^2}{8\pi G(t)} \ln(tH) - \rho_D (\ln(tH) - \sin\left(t \frac{\dot{G}(t)}{G(t)}\right)) \right). \quad (30)$$

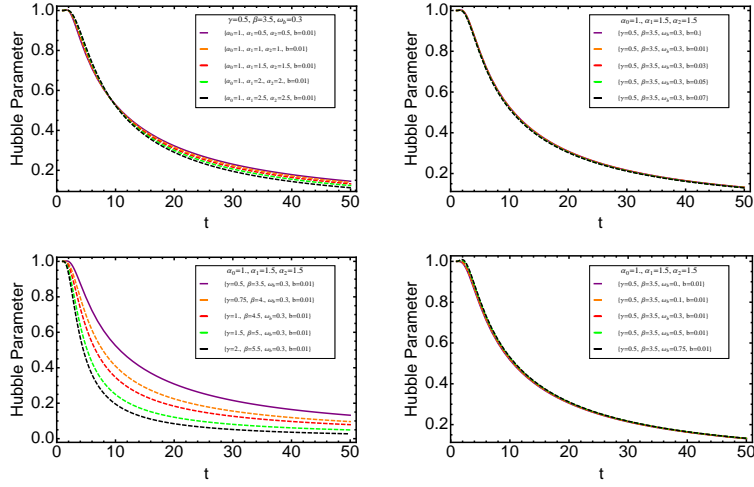
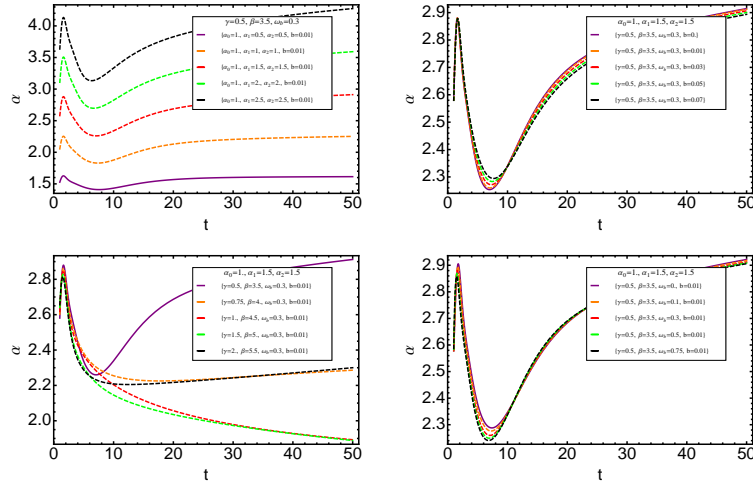
$$\frac{\dot{G}(t)}{G(t)} + \frac{\dot{\Lambda}(t)}{3H^2 - \Lambda(t)} = 0. \quad (31)$$

FIG. 7: Behavior of $\dot{G}(t)/G(t)$ against t for Model 1.FIG. 8: Behavior of Gravitational constant $G(t)$ against t Model 2.

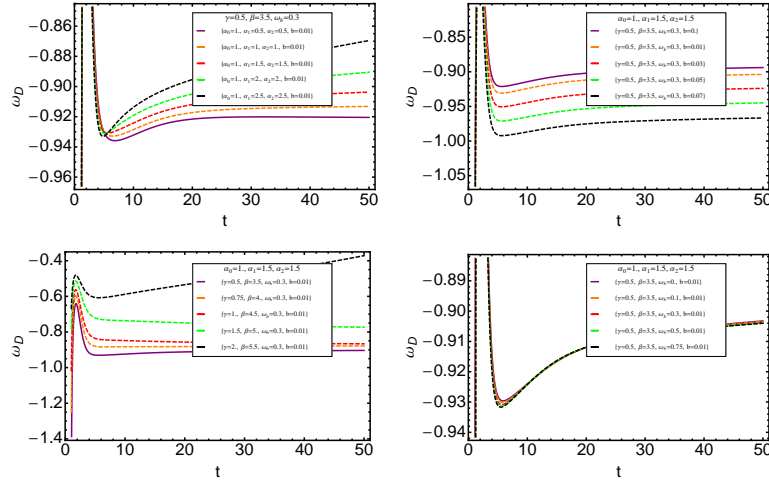
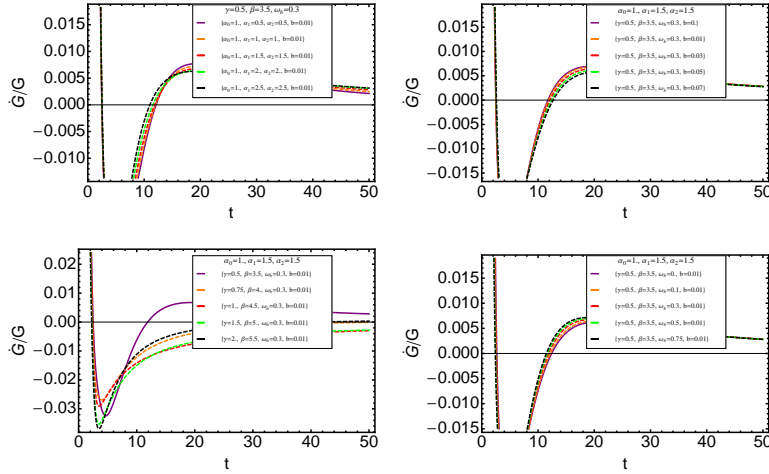
Equation (31) with (30) will give us the behavior of $G(t)$. This model also includes several interesting facts about the behavior of the cosmological parameters. After recovering the $G(t)$ we observe that $G(t)$ is an increasing function, and its graphical behavior for the different cases are given in Fig.(15). For instance with increasing β and γ with $\alpha_0 = \alpha_2 = 1$, $\alpha_1 = 1.5$, $\omega_b = 0.3$ and $b = 0.01$ we have the following picture: $\gamma = 0.1$ and $\beta = 2.5$ (a blue line at left-bottom plot) we have a decreasing behavior for $G(t)$, while for the higher values for γ and β we have increasing behavior for later stages of evolution. With increasing ω_b we decrease the value of $G(t)$ (right-bottom). We also observe that there is a period in history of the evolution where $G(t)$ can be a constant. With $\alpha_0 = \alpha_2 = 1$, $\alpha_1 = 1.5$, $\gamma = 0.5$, $\beta = 3.5$ and $\omega_b = 0.3$ we see that for non interacting case, when $b = 0$ (a blue

FIG. 9: Behavior of EoS parameter ω_{tot} against t for Model 2.FIG. 10: Behavior of deceleration parameter q against t for Model 2.

line at right-top plot) at later stages of evolution $G(t) = \text{const} \approx 1.36$, while when we include the interaction and increase the value of b , increase in the value of $G(t)$ is observed. Behavior of $G(t)$ from α_0 , α_1 and α_2 can be found at the left-top plot of Fig.(15). Other cosmological parameter that we have investigated for this model is a ω_{tot} describing interacting DE and DM two component fluid model. From Fig.(16) we can make conclusion about the behavior of the parameter. We observe that as a function of α_0 , α_1 and α_2 , while the other parameters are being fixed, we have a decreasing function for the initial stages of evolution, while for the later stages we have a constant value for ω_{tot} . With increasing α_1 and α_2 we will increase ω_{tot} and we have a possibility to obtain decreasing-increasing-constant behavior (left-top plot). On the right-top plot we see the role of the interaction

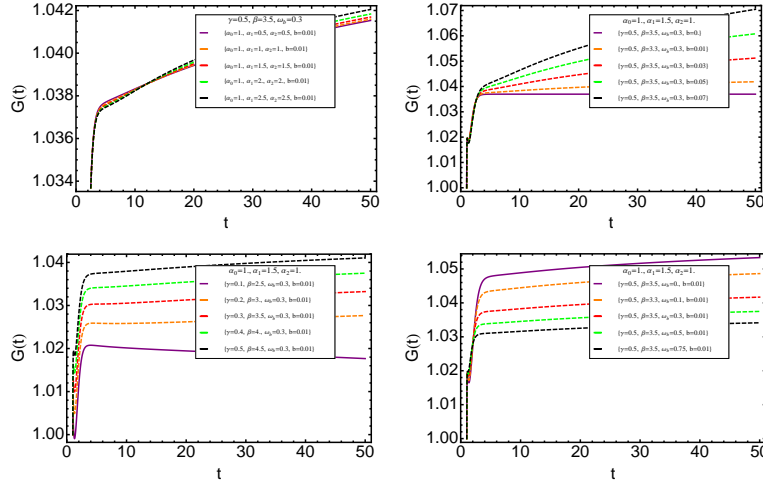
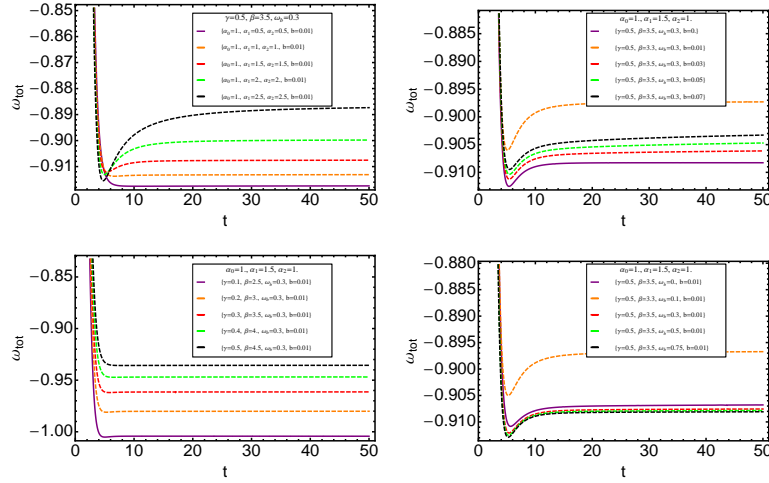
FIG. 11: Behavior of Hubble parameter $H(t)$ versus t for Model 2.FIG. 12: Behavior of α versus t for Model 2.

Q . Starting with the non interacting case $b = 0$ and increasing b we observe the increasing value of ω_{tot} . Bottom panel of Fig.16 represents graphical behavior of ω_{tot} from $\{\gamma, \beta\}$ and ω_b . The last parameter discussed in this section will be the deceleration parameter q recovered for this specific $\Lambda(t)$. Investigating the behavior we conclude that for this model, $\gamma > 0.1$ and $\beta > 2.5$ should be taken in order to get $q > -1$ (Fig.(17) left-bottom plot). It starts its evolution from -1 and then it is strictly $q > -1$ for later stages of evolution. Interaction as well as ω_b has a small impact on the behavior of q . Left-top plot of Fig.17 represents the behavior of q as a function of α_0 , α_1 and α_2 . As for the other models, additional information about other cosmological parameters of this model can be found in Appendix.

FIG. 13: Behavior of ω_D against t for Model 2.FIG. 14: Behavior of $\dot{G}(t)/G(t)$ against t for Model 2.

V. STATE FINDER DIAGNOSTIC

In the framework of GR, Dark energy can explain the present cosmic acceleration. Except cosmological constant many other candidates of dark energy (quintom, quintessence, brane, modified gravity etc.) are proposed. Dark energy is model dependent and to differentiate different models of dark energy, a sensitive diagnostic tool is needed. Since $\dot{a} > 0$, hence $H > 0$ means the expansion of the universe. Also, $\ddot{a} > 0$ implies $q < 0$. Since, the various dark energy models give $H > 0$ and $q < 0$, they cannot provide enough evidence to differentiate the more accurate cosmological observational data and the more general models of dark energy. For this aim we need higher order of time

FIG. 15: Behavior of Gravitational constant $G(t)$ against t Model 3.FIG. 16: Behavior of EoS parameter ω_{tot} against t for Model 3.

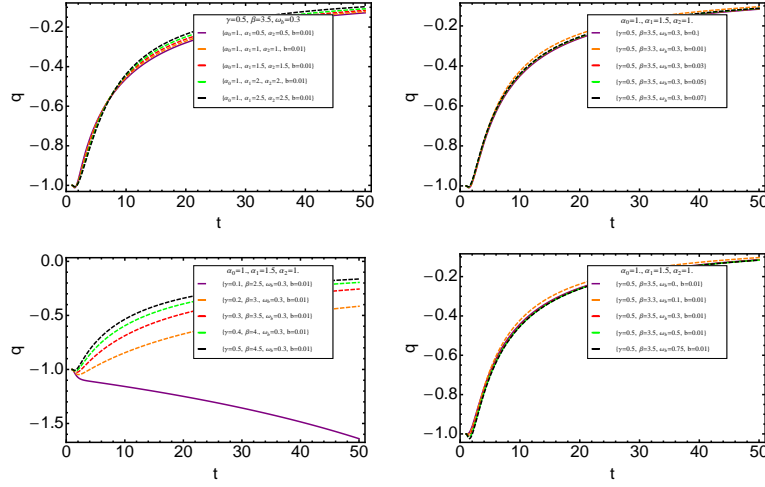
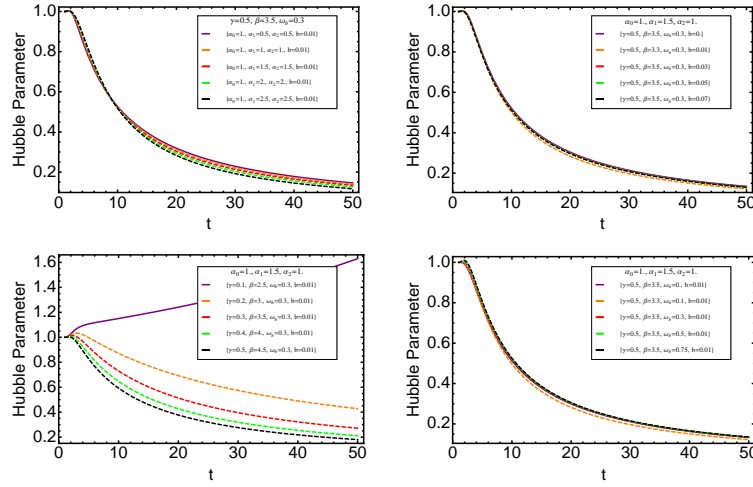
derivative of scale factor and geometrical tool. Sahni *et.al.* [36] proposed geometrical statefinder diagnostic tool, based on dimensionless parameters (r, s) which are function of scale factor and its time derivative. These parameters are defined as

$$r = \frac{1}{H^3} \frac{\ddot{a}}{a} \quad s = \frac{r - 1}{3(q - \frac{1}{2})}. \quad (32)$$

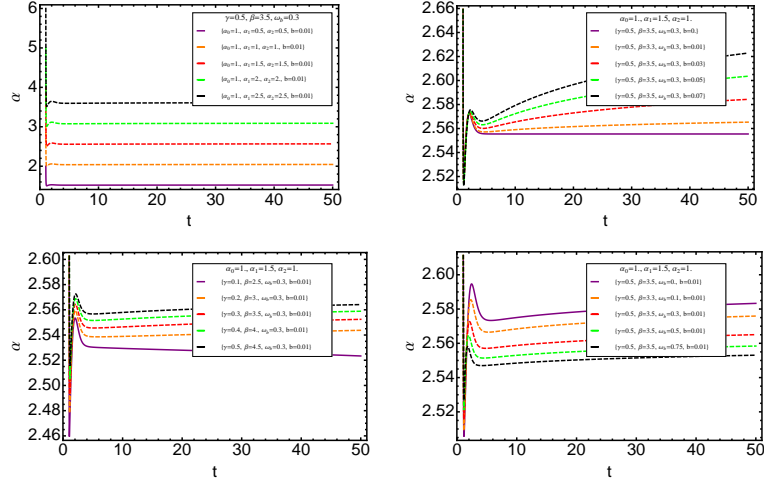
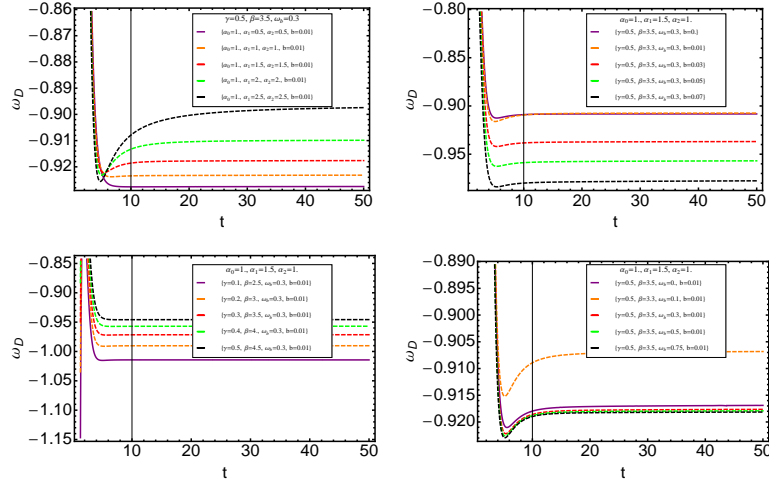
For $8\pi G = 1$ and $\Lambda = 0$ we can obtain another form of parameters r and s :

$$r = 1 + \frac{9(\rho + P)}{2\rho} \frac{\dot{P}}{\dot{\rho}}, \quad s = \frac{(\rho + P)}{P} \frac{\dot{P}}{\dot{\rho}}. \quad (33)$$

For the model 3 of our consideration, we presented the $\{r, s\}$ in Fig.(22) as a function of β and γ .

FIG. 17: Behavior of deceleration parameter q against t for Model 3.FIG. 18: Behavior of Hubble parameter $H(t)$ against t for Model 3.

As we know the pair $\{r, s\} = \{1, 0\}$ corresponds to the Λ CDM model. It is indicated on our graphs for both models. Further, $\{1, 0\}$ which shows the CDM model, is present in our models. But we observe the absence of Einstein static universe due to this fact that our models never mimic the pair $\{-\infty, +\infty\}$. So, our models fit the Λ CDM and CDM perfectly.

FIG. 19: Behavior of α against t for Model 3.FIG. 20: Behavior of ω_D against t for Model 3.

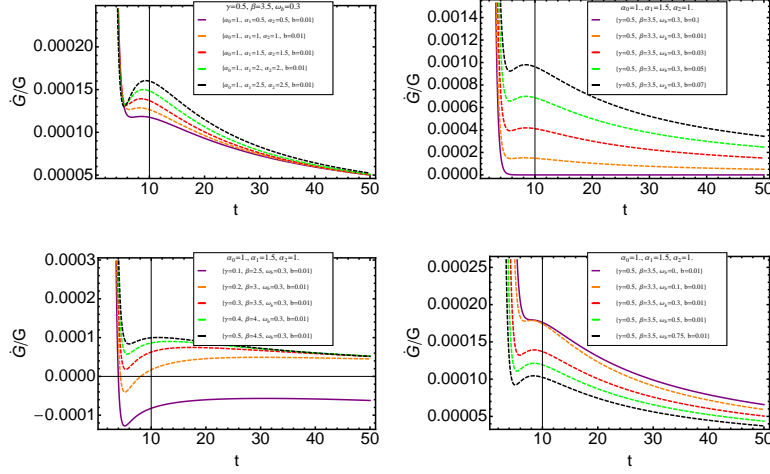
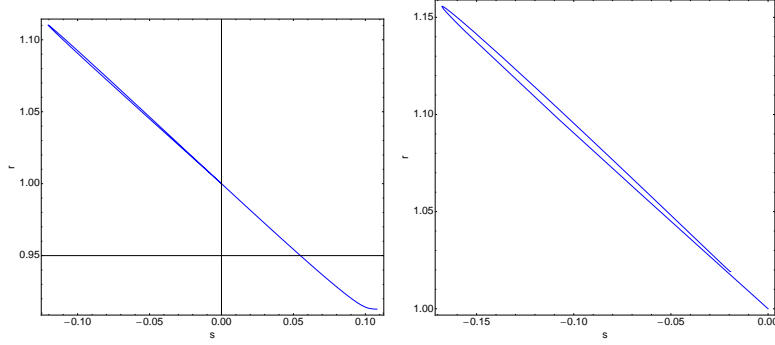
VI. OBSERVATIONAL CONSTRAINTS

To use the *SNIa* data, we define distance modulus μ as a function of the luminosity distance D_L as the following:

$$\mu = m - M = 5 \log_{10} D_L, \quad (34)$$

Here D_L is in the following form:

$$D_L = (1+z) \frac{c}{H_0} \int_0^z \frac{dz'}{\sqrt{H(z')}}. \quad (35)$$

FIG. 21: Behavior of $\dot{G}(t)/G(t)$ against t for Model 3.FIG. 22: r - s for model 3. $\beta = 2.5$ and $\gamma = 0.1$ for the left plot. $\beta = 3.5$ and $\gamma = 0.3$ for the right plot. $\alpha_0 = 1.0$, $\alpha_1 = 1.5$, $\alpha_2 = 1.0$, $\omega_b = 0.3$ and $b = 0.01$.

Here m and M denote the apparent magnitude and absolute magnitude, respectively. Due to the photon-baryon plasma, Baryonic acoustic oscillations exist in the decoupling redshift $z = 1.090$. A major for scaling is the following quantity

$$A = \frac{\sqrt{\Omega_{m0}}}{H(z_b)^{1/3}} \left[\frac{1}{z_b} \int_0^{z_b} \frac{dz}{H(z)} \right]^{2/3}. \quad (36)$$

From WiggleZ-data [37] we know that $A = 0.474 \pm 0.034$, 0.442 ± 0.020 and 0.424 ± 0.021 at the redshifts $z_b = 0.44$, 0.60 and 0.73 . The major statistical analysis parameter is:

$$\chi^2(x^j) = \sum_i^n \frac{(f(x^j)_i^t - f(x^j)_i^0)^2}{\sigma_i}, \quad (37)$$

Here $f(x^j)_i^t$ is the theoretical function of the model's parameters. To conclude the work and model analysis we perform comparison of our results with observational data. SNeIa data allowed us to

obtain the following observational constraints for our models. For the Model 1, we found that the best fit can occurred with $\Omega_{m0} = 0.24$ and $H_0 = 0.3$. For $\alpha_0 = 0.3$, $\alpha_1 = 0.5$, $\alpha_2 = 0.4$ and $\beta = 4.0$, $\gamma = 1.4$, $\omega_b = 0.5$, while for interaction parameter $b = 0.02$. For the Model 2, we found that the best fit we can obtain with $H_0 = 0.5$ and $\Omega_m = 0.4$. Meanwhile for $\alpha_0 = 1.0$, $\alpha_1 = 1.5$, $\alpha_2 = 1.3$ and $\beta = 3.5$, $\gamma = 0.5$, $\omega_b = 0.3$, while for interaction parameter $b = 0.01$. Finally we present the results obtained for Model 3, which say that the best fit is possible when $H_0 = 0.35$ and $\Omega_{m0} = 0.28$. For the parameters α_0 , α_1 , α_2 , β , γ , ω_b and b we have the numbers 0.7, 1.0, 1.2, 3, 0.8, 0.75 and 0.01 respectively. Finally, we would like to discuss the constraints resulted from *SNeIa + BAO + CMB* [35] .

M	α_0	α_1	α_2	β	γ	ω_b	b	H_0	Ω_{m0}
1	$0.3^{+0.35}_{-0.15}$	$0.5^{+0.35}_{-0.4}$	$0.4^{+0.35}_{-0.1}$	$4.0^{+1.3}_{-2.7}$	$1.4^{+0.25}_{-0.25}$	$0.5^{+0.4}_{-0.5}$	$0.01^{+0.07}_{-0.01}$	$0.25^{+0.35}_{-0.05}$	$0.26^{+0.04}_{-0.03}$
2	$1.2^{+0.2}_{-0.5}$	$1.1^{+0.4}_{-0.3}$	$0.7^{+0.55}_{-0.15}$	$3.0^{+1.5}_{-0.8}$	$0.7^{+0.12}_{-0.3}$	$0.4^{+0.6}_{-0.2}$	$0.02^{+0.03}_{-0.005}$	$0.4^{+0.35}_{-0.2}$	$0.3^{+0.2}_{-0.05}$
3	$0.7^{+0.5}_{-0.3}$	$1.0^{+0.2}_{-0.4}$	$1^{+0.1}_{-0.3}$	$3.0^{+1.0}_{-0.3}$	$0.8^{+0.1}_{-0.4}$	$0.7^{+0.6}_{-0.1}$	$0.01^{+0.09}_{-0.01}$	$0.3^{+0.3}_{-0.1}$	$0.21^{+0.15}_{-0.01}$

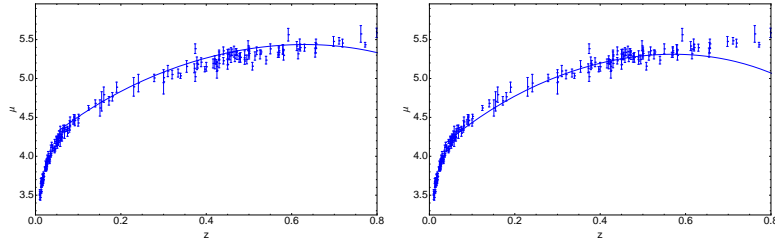


FIG. 23: Observational data *SneIa + BAO + CMB* for distance modulus versus our theoretical results for models 1 and 2.

From the graph of luminosity distance versus zm we learn that how μ depends on the values of the parameters for different redshifts z . For different values of $\Omega_M, \Omega_D = 0$ and in the regime of low redshifts $0.001 < z < 0.01$, this graph has linearity. For $z > 0.4$ the graph has typical form of models with Ω_M . Hubble parameter H has a central role in the behavior of $\mu(z)$ for different ranges of z . We can use it to investigate the cosmological parameters.

VII. SUMMARY

Time varying cosmological models with gravitational and cosmological constant have been studied frequently. Nevertheless, in view of cosmological data, rate of change of G is small. So the first order correction terms are more important. Our approach to $\Lambda(t), G(t)$ models is slightly different and more general than any other previous work. As a proper generalization of general relativity, scalar-tensor-vector gravity model has been proposed to explain the structure of galaxies and dark matter problem. If we assume small changes in the variation of the scalar fields, MOG model at the level of action becomes equivalent to Einstein-Hilbert model, of course it is necessary that we consider $G(t)$ as a slowly varying scalar field. We proposed three models of generalized Ricci dark energy including $\Lambda(t), G(t)$ to complete the time evolution of dark energy. Due to the complexity of the model equations, the numerical algorithms with cosmological parameters have been used. Gravitational acceleration region and time evolution of state finder parameters $\{r, s\}$ compared with Λ CDM model are numerically studied with high accuracy. We obtained the fit range of data models by comparing the free parameters of dark energy models and cosmological data $SNeIa + BAO + CMB$. Our model is a model that is consistent with cosmological data while the other theoretical models are not.

Acknowledgments

The authors thank J.W.Moffat for useful comments about MOG.

-
- [1] A.G. Riess, et al., Astron. J. 116 (1998) 1009 [astro-ph/ 9805201]; S. Perlmutter, et al., Astrophys. J. 517 (1999) 565 [astro-ph/9812133]; C.L. Bennett, et al., Astrophys. J. Suppl. 148 (2003) 1 [astro-ph/0302207]; D.N. Spergel, et al., Astrophys. J. Suppl. 148 (2003) 175 [astro-ph/0302209]; M. Tegmark, et al., Phys. Rev. D 69 (2004) 103501 [astro-ph/0310723]; K. Abazajian, et al., [astro-ph/0410239]; K. Abazajian, et al., Astron. J. 128 (2004) 502 [astro-ph/0403325]; K. Abazajian, et al., Astron. J. 126 (2003) 2081 [astro-ph/0305492]; E. Hawkins, et al., Mon. Not. Roy. Astron. Soc. 346 (2003) 78 [astro-ph/0212375]; L. Verde, et al., Mon. Not. Roy. Astron. Soc. 335 (2002) 432 [astro-ph/0112161]
 - [2] K. Bamba, S. 'i. Nojiri and S. D. Odintsov, arXiv:1302.4831 [gr-qc].
 - [3] M. Sami and R. Myrzakulov, arXiv:1309.4188 [hep-th].
 - [4] M. Jamil, F. Rahaman and M. Kalam, Eur. Phys. J. C **60**, 149 (2009) [arXiv:0809.4314 [gr-qc]].
 - [5] M. R. Setare and M. Jamil, Gen. Rel. Grav. **43**, 293 (2011) [arXiv:1008.4763 [gr-qc]].

- [6] M. Jamil and U. Debnath, *Int. J. Theor. Phys.* **50**, 1602 (2011) [arXiv:0909.3689 [gr-qc]].
- [7] M. Jamil, *Int. J. Theor. Phys.* **49**:2829-2840, 2010, arXiv:1010.0158 [astro-ph.CO].
- [8] M. Jamil et al., *Astrophys. Space Sci.* (2012) 337:799-803, arXiv:1110.4053 [physics.gen-ph].
- [9] M. R. Setare and M. Jamil, *JCAP* **1002**, 010 (2010) [Erratum-ibid. **1008**, E01 (2010)] [arXiv:1001.1251 [hep-th]].
- [10] Shuvendu Chakraborty, Ujjal Debnath, Mubasher Jamil, Ratbay Myrzakulov, *Int. J. Theor. Phys.* (2012) 51:2246-2255, arXiv:1111.3853 [physics.gen-ph].
- [11] H. A. Buchdahl, *Mon. Not. Roy. Astron. Soc.*, **150**, 1 (1970).
- [12] H. Motohashi, A. A. Starobinsky and J. 'i. Yokoyama, *Int. J. Mod. Phys. D* **20**, 1347 (2011) [arXiv:1101.0716 [astro-ph.CO]].
- [13] H. Motohashi, A. A. Starobinsky and J. 'i. Yokoyama, *Prog. Theor. Phys.* **123**, 887 (2010) [arXiv:1002.1141 [astro-ph.CO]].
- [14] H. Motohashi, A. A. Starobinsky and J. 'i. Yokoyama, arXiv:1002.0462 [astro-ph.CO].
- [15] S. A. Appleby, R. A. Battye and A. A. Starobinsky, *JCAP* **1006**, 005 (2010) [arXiv:0909.1737 [astro-ph.CO]].
- [16] A. A. Starobinsky, *JETP Lett.* **86**, 157 (2007) [arXiv:0706.2041 [astro-ph]].
- [17] C. Kiefer, F. Queisser and A. A. Starobinsky, *Class. Quant. Grav.* **28**, 125022 (2011) [arXiv:1010.5331 [astro-ph.CO]].
- [18] A. Shafieloo, V. Sahni and A. A. Starobinsky, *Phys. Rev. D* **80**, 101301 (2009) [arXiv:0903.5141 [astro-ph.CO]].
- [19] V. Sahni, A. Shafieloo and A. A. Starobinsky, *Phys. Rev. D* **78**, 103502 (2008) [arXiv:0807.3548 [astro-ph]].
- [20] U. Alam, V. Sahni and A. A. Starobinsky, *JCAP* **0406**, 008 (2004) [astro-ph/0403687].
- [21] V. Sahni and A. Starobinsky, *Int. J. Mod. Phys. D* **15**, 2105 (2006) [astro-ph/0610026].
- [22] R. Gannouji, D. Polarski, A. Ranquet and A. A. Starobinsky, *JCAP* **0609**, 016 (2006) [astro-ph/0606287].
- [23] R. Gannouji, D. Polarski, A. Ranquet and A. A. Starobinsky, astro-ph/0701650.
- [24] J. W. Moffat, *JCAP*, 0603 ,004(2006).
- [25] J. W. Moffat and V. T. Toth, *Galaxies* **1**, 65 (2013) [arXiv:1104.2957 [astro-ph.CO]].
- [26] V. T. Toth, arXiv:1011.5174 [gr-qc].
- [27] J. W. Moffat and V. T. Toth, arXiv:0710.0364 [astro-ph].
- [28] A. Bonanno, G. Esposito, C. Rubano and P. Scudellaro, *Class. Quant. Grav.* **24**, 1443 (2007) [gr-qc/0610012].
- [29] Abdussattar and R. G. Vishwakarma, *Class. Quant. Grav.* **14**, 945 (1997).
- [30] M. Jamil, E. N. Saridakis and M. R. Setare, *Phys. Lett. B* **679**, 172 (2009) [arXiv:0906.2847 [hep-th]].
- [31] J. Lu, E. N. Saridakis, M. R. Setare and L. Xu, *JCAP* **1003**, 031 (2010) [arXiv:0912.0923 [astro-ph.CO]].
- [32] J. Sadeghi, M. Khurshudyan, A. Movsisyan and H. Farahani, *JCAP* **1312**, 031 (2013) [arXiv:1308.3450 [gr-qc]].
- [33] S. Chen, J. Jing, *Phys. Lett. B*, **679**, 144 (2009)

- [34] S. del Campo, J. . C. Fabris, R. nHerrera and W. Zimdahl, arXiv:1303.3436 [astro-ph.CO].
- [35] D. J. Eisenstein, et al., *Astrophys. J.* 633, 560 (2005); Y. Wang and P. Mukherjee, *Astrophys. J.* 650, 1 (2006); J. R. Bond, G. Efstathiou and M. Tegmark, *Mon. Not. Roy. Astron. Soc.* 291, L33 (1997).
- [36] V. Sahni, T. D. Saini, A. A. Starobinsky, and U. Alam, Statefinder – a new geometrical diagnostic of dark energy, *JETP Lett.* **77**, 201 (2003).
- [37] C. Blake et al, The WiggleZ Dark Energy Survey: mapping the distance-redshift relation with baryon acoustic oscillations, arXiv:1108.2635.